NANO LETTERS
Letter
Cite This: Nano Lett. 2019, 19, 4420−4426
pubs.acs.org/NanoLett

Large Tunable Spin-to-Charge Conversion Induced by Hybrid Rashba and Dirac Surface States in Topological Insulator Heterostructures

Rui Sun,[†,§] Shijia Yang,[‡] Xu Yang,[†,§] Eric Vetter,[‡] Dali Sun,[*,‡] Na Li,[†,§] Lei Su,[†,§] Yan Li,[†,§] Yang Li,[†,§] Zi-zhao Gong,[†,§] Zong-kai Xie,[†,§] Kai-yue Hou,[†] Qeemat Gul,[†,§] Wei He,[†] Xiang-qun Zhang,[†] and Zhao-hua Cheng[*,†,§,∥]

[†]State Key Laboratory of Magnetism and Beijing National Laboratory for Condensed Matter Physics, Institute of Physics, Chinese Academy of Sciences, Beijing 100190, China

[‡]Department of Physics, North Carolina State University, Raleigh, North Carolina 27695, United States

[§]School of Physical Sciences, University of Chinese Academy of Sciences, Beijing 100049, China

[∥]Songshan Lake Materials Laboratory, Dongguan, Guangdong 523808, China

Supporting Information

ABSTRACT: Topological insulators (TIs) have emerged as some of the most efficient spin-to-charge convertors because of their correlated spin-momentum locking at helical Dirac surface states. While endeavors have been made to pursue large "charge-to-spin" conversions in novel TI materials using spin-torque-transfer geometries, the reciprocal process "spin-to-charge" conversion, characterized by the inverse Edelstein effect length (λ_{IEE}) in the prototypical TI material (Bi_2Se_3), remains moderate. Here, we demonstrate that, by incorporating a "second" spin-splitting band, namely, a Rashba interface formed by inserting a bismuth interlayer between the ferromagnet and the Bi_2Se_3 (i.e., ferromagnet/Bi/Bi_2Se_3 heterostructure), λ_{IEE} shows a pronounced increase (up to 280 pm) compared with that in pure TIs. We found that λ_{IEE} alters as a function of bismuth interlayer thickness, suggesting a new degree of freedom to manipulate λ_{IEE} by engineering the interplay of Rashba and Dirac surface states. Our finding launches a new route for designing TI- and Rashba-type quantum materials for next-generation spintronic applications.

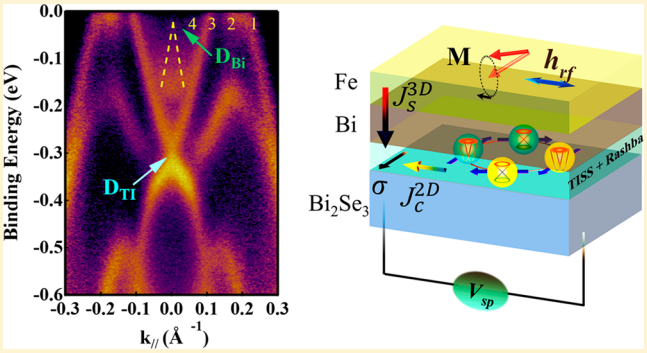

KEYWORDS: *Spintronics, topological insulator, topological insulator junction, inverse Edelstein effect, Rashba surface state, spin−charge conversion*

A key goal of spintronics is to achieve high spin−charge interconversions at room temperature for future spin logic and computing applications. The topological insulator (TI)—a nontrivial quantum matter—intriguingly exhibits both bulk-insulating and surface-conducting states that are topologically protected by time-reversal symmetry[1,2] as well as possesses efficient spin−charge interconversion.[3,4] In the presence of a strong spin−orbit interaction, the TI surface state (TISS) forms two spin-split bands and results in a strong correlated "spin-momentum locking" Dirac surface state with clockwise (counterclockwise) spin helicity Fermi contours above (below) the Dirac point (Figure 1a). When a nonzero three-dimensional (3D) spin current j_s^{3D} (spin polarization along *y*-direction) is injected into the Dirac surface state from an adjacent ferromagnetic (FM) layer, a transverse 2D charge current (j_c^{2D}) will be generated along the *x*-direction via the inverse Edelstein effect (IEE) or vice versa (Figure 1a).[5] The efficiency of this spin-to-charge conversion, represented by the IEE length ($\lambda_{IEE}(TI) = j_c^{2D}/j_s^{3D}$, in the unit of length), is expressed as $\lambda_{IEE}(TI) = \nu_F\tau_s$, where ν_F is the Fermi velocity of Dirac fermions, and τ_s is the effective spin-momentum scattering time at the Fermi contour.[5,6] It is found that the IEE length at the TISS can be orders of magnitude larger than that in conventional heavy metals via the inverse spin Hall effect,[4,7] making TI materials promising candidates for efficient spin-to-charge convertors at room temperature.[8]

In addition to the IEE conversion via TISS, Rashba spin-splitting bands formed at the two-dimensional electron gas (2DEG) also exhibit an efficient spin-to-charge interconversion.[8,9] At the Rashba interface, the spin and momentum are tightly correlated and form two degenerate spin contours with opposite helicity because of broken inversion symmetry

Received: March 20, 2019
Revised: May 16, 2019
Published: May 28, 2019

DOI: 10.1021/acs.nanolett.9b01151
Nano Lett. 2019, 19, 4420−4426

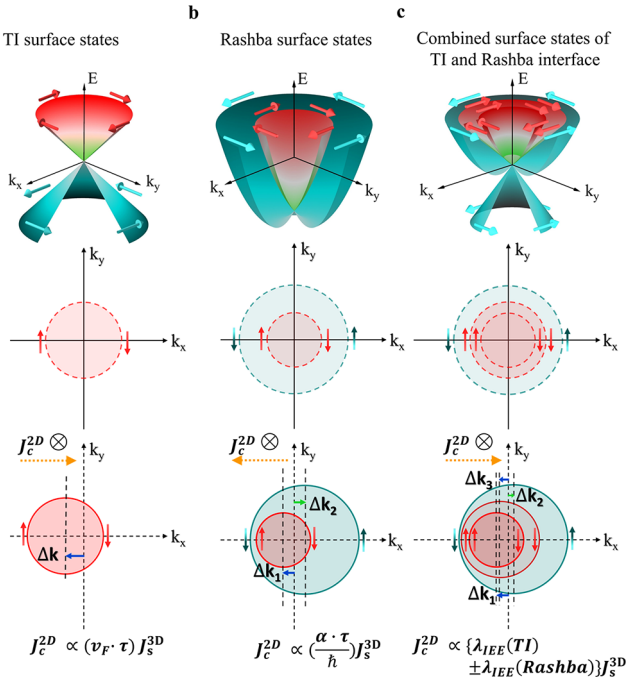

Figure 1. Illustration of the concept of spin-to-charge conversion via inverse Edelstein effect (IEE) at a topological surface, two-dimensional electron gas state, and their hybrid state. Top panels: schematic illustration of the energy dispersion of (a) the topological surface state (TISS) of a topological insulator (TI), (b) Rashba spin-splitting bands at a two-dimensional electron gas (2DEG) interface with two contours with helical spin configuration of opposite helicity, and (c) TISS and Rashba hybrid bands due to the formation of a 2DEG interface at the surface of TI. Middle panels: schematic view of the in-plane component of the spin texture at the Fermi surface of three systems. The red and black−green arrows represent the spin angular momenta with opposite helicity. Bottom panels: IEE in the three systems. The injection of a 3D spin current (J_s^{3D}) with spin polarization density along the +y-direction leads to an imbalance of population on one side of the Fermi contour (here along the x-direction), generating a 2D horizontal charge current density, J_c^{2D}. The directions of charge current density are drawn in such a way that all three systems possess the same sign of spin-to-charge conversion efficiency while the Rashba coefficient (α_R) and Fermi velocity (v_F) have the same polarity. Notably, in a Rashba state or hybrid states, there is partial compensation of the opposite contributions of the two contours that may decrease the spin-to-charge conversion efficiency.

(Figure 1b).[9] The spin-to-charge conversion efficiency at this 2DEG interface can be written as $\lambda_{IEE}(\text{Rashba}) = j_c^{2D}/j_s^{3D} = \alpha_R\tau_s/\hbar$, where α_R is the Rashba coefficient.[6,10] Interestingly, the TISS inherently generates a 2DEG state with pronounced Rashba-split bands[11,12] when attached to strong spin−orbit coupling materials such as bismuth,[13] graphene,[14] and WSe_2.[15] In addition, when one bilayer of bismuth (predicted as a 2D-type TI material[16]) is deposited on top of a 3D-type TI Bi_2Se_3, the strong potential gradient at the Bi/Bi_2Se_3 interface gives rise to a new type of helical Dirac surface state (DSS) via the topological proximity effect.[17] This emergent Rashba coefficient α_R would reach up to 4 eV·Å,[18] which is larger than that in the prototypical 2DEG Ag/Bi system (3 eV·Å).[19] Thus, we envision that if the spin current j_s^{3D} is injected into such a hybrid interface containing both TISS and Rashba states, the combined spin-to-charge conversion efficiency would be enhanced due to their synergistic contributions (Figure 1c). In contrast to the energy-independent Fermi velocity (v_F) and net spin polarization at the TISS, the Rashba-induced net spin polarization is energy-dependent,[20] indicating that the λ_{IEE}(Rashba) may be altered by shifting the position of the Fermi level with charge transfer induced from the bismuth layer to bismuth selenide layer, or from the gradient of charge potential induced from the metal top-layers.[21]

Here, we report the observation of large tunable spin-to-charge conversion in the Fe/Bi(n)/Bi_2Se_3 heterostructure due to the combined TISS and Rashba states (n is the number of Bi bilayers deposited on top of the 3D-TI Bi_2Se_3 thin film). The obtained IEE length (∼280 pm) in the Fe/Bi(5BL)/Bi_2Se_3(9QL) heterostructure is about 5 times greater than that in the prototypical FM/Bi_2Se_3 system (reported λ_{IEE} varies between 35 pm[4] to 70 pm[22]). In situ angle-resolved photoemission spectroscopy (ARPES) validates the formation of TISS−Rashba hybrid bands at the Bi/Bi_2Se_3 interface and the shift of Fermi level by changing the thickness of the Bi bilayer via surface electron doping induced by the charge transfer effect. By performing ferromagnetic resonance (FMR) and spin pumping measurements, we found that the shift of Fermi level leads to a systematic change of the IEE length in the Fe/Bi(n)/Bi_2Se_3 heterostructures. This is usually inaccessible by applying an external gate voltage that merely acts on the bottom TISS state of the TIs.[23,24] Our study opens a new avenue to design novel 2DEG/TI-based quantum spintronic devices.

Angle-Resolved Photoemission Spectroscopy Characterization. Figure 2b shows the obtained energy dispersion of the as-grown Bi_2Se_3 thin film (see the Supporting Information), exhibiting a perfect linearly dispersing TISS with well-defined Dirac cone (D_{TI}) at 293 meV below the Fermi level. The visible bulk valence bands at higher binding energy are due to the usual degenerate electron doping.[25] From the measured energy dispersion, the Fermi velocity $v_F \sim 5.14 \times 10^5$ m/s can be determined, consistent with previous experimental reports.[26]

By adding one bilayer of Bi on top of the Bi_2Se_3 thin film, the position of D_{TI} shifts toward higher binding energy (down to −310 meV). This suggests a charge transfer from the Bi bilayer to the top-QL Bi_2Se_3 associated with increased surface electron doping,[27] resulting in the formation of a two-dimensional electron gas (2DEG) at the interface between Bi and the top-QL Bi_2Se_3.[18] This added 2DEG electronic state produces a new Rashba-like Dirac cone due to the large spin−orbit coupling and broken inversion symmetry at the 2DEG. This Dirac cone (DC) D_{Bi} (indicated by sub-band "4" in Figure 2c) was located around 20 meV below the Fermi level, which is consistent with previous reports.[18,21,26] In addition, two distinguishable bands appear outside the TISS states (sub-bands "1" and "2"), indicating a Rashba-type spin splitting due to a lack of inversion symmetry at the two-dimensional limit.[18,21,26] According to previous theoretical calculations in ref 18, this Rashba spin-splitting coefficient (α_R) could be as large as ∼4 eV·Å.[18] Notably, the TISS from the Bi_2Se_3 surface state is clearly visible, while the Fermi velocity is reduced to 3.81×10^5 m/s. Figure 2e,f shows the Fermi contour of the Bi(1BL)/Bi_2Se_3 multilayer using in situ ARPES spectroscopy, from which four sub-bands are observed. The generation of the hybrid dual DSS (D_{TI} and D_{Bi}) and Rashba states is mainly attributed to the hybridization between the Bi layer and the bulk states of Bi_2Se_3.[18] Inferred by previous theoretical calculations,[18,26] the predicated spin texture of Fermi contour has also been schematically illustrated in Figure 2f. The

DOI: 10.1021/acs.nanolett.9b01151
Nano Lett. 2019, 19, 4420−4426

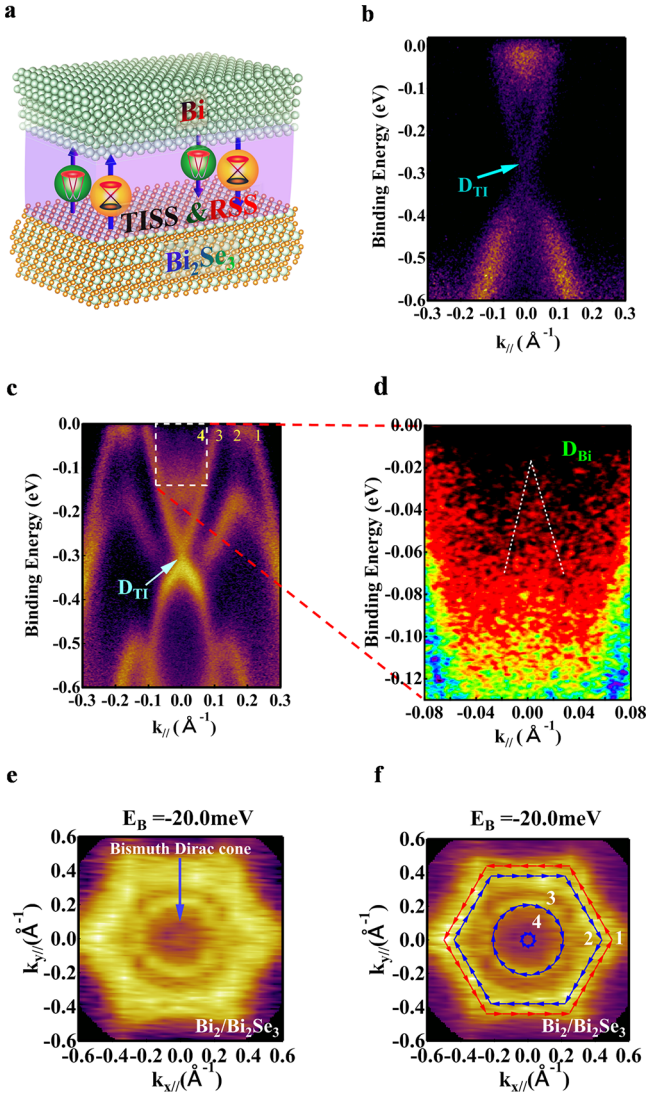

Figure 2. (a) Illustration of the hybrid states formed between bismuth and bismuth selenide. (b, c) Energy dispersion at the surface of as-grown Bi_2Se_3(9QL) and Bi(1BL)/Bi_2Se_3(9QL) thin film, respectively. The cyan arrow indicates the TISS (labeled as band "3"), and the different Rashba-induced sub-bands can be distinguished (labeled as sub-band "1", "2", and "4"). $k_{\parallel}$ is along the $\Gamma-K$ direction. (d) Zoomed in areas in part c. The "Λ" dashed lines are a guide for the eyes, depicting the position of the Dirac cone from bismuth (D_{Bi}). (e) Energy contour around the Fermi Level in the Bi(1BL)/Bi_2Se_3(9QL) thin film. The light blue arrow points the existence of Dirac cone from bismuth. (f) Corresponding spin texture around the Fermi surface in Bi(1BL)/Bi_2Se_3(9QL) thin film. The red (blue) arrows indicate the calculated counterclockwise (clockwise) spin texture at each band.

outmost hexagonal Fermi contour (band "1") with right-handed spin helicity and the inner circle Fermi contour (band "2") with left-handed spin helicity are attributed to the Rashba-split sub-bands. The second DC from the Bloch state in the Bi bilayer (band "4") located at the center of the Fermi contour shows the same spin helicity[18,26] as the original DC (band "3") from the TISS in the top-QL Bi_2Se_3. As mentioned above, the mechanism that the surface electron doping comes about by the charge transfer from the bismuth to the Bi_2Se_3 layer was confirmed by both theoretical calculations and ARPES measurements.[18,26,27] With more surface electron doping by adding Bi bilayers, the Fermi level will be lifted up so that D_{TI} will show a further downward shift.[18] The coexistence of dual DSSs and Rashba states can still be preserved when the interface of the Bi/Bi_2Se_3 is buried below thick Bi bilayers, although the contrast of the intensity for each band is weak.

Ferromagnetic Resonance Characterization. A schematic view of the device structure used for ferromagnetic resonance (FMR) and spin pumping measurements is shown in Figure 3a. Figure 3b shows typical magnetic field dependence of FMR derivative spectra in Fe/MgO, Fe/Bi_2Se_3(9QL) and Fe/Bi(1BL)/Bi_2Se_3(9QL) samples. Figure 3c shows the microwave frequency (f) dependence of the full width half-maximum, $\mu_0\Delta H$, that was extracted by fitting the FMR spectra in Fe/MgO, Fe/Bi(1BL)/Al_2O_3, Fe/Bi_2Se_3(9QL)/$SrTiO_3$, and Fe/Bi(1BL)/Bi_2Se_3(9QL)/$SrTiO_3$ samples. The slope of $\mu_0\Delta H(f)$ for Fe/Bi(1BL)/Bi_2Se_3(9QL), which is proportional to the damping factor, $\alpha_{F/N}$, is significantly larger than that for the Fe/MgO sample. The increase of the damping factor provides direct evidence of spin injection from the Fe layer into a hybrid TI and Rashba system via spin pumping.

By inserting only one bilayer of Bi between Fe and Bi_2Se_3, the value of the damping factor for the Fe/Bi(1BL)/Bi_2Se_3(9QL) sample is 0.060 ± 0.007, which is about 2 times larger than that of the Fe/Bi_2Se_3 and Fe/Bi(1BL)/Al_2O_3 (~0.030 ± 0.001). This increase can be attributed to the enhanced spin mixing conductance ($g_{eff}^{\uparrow\downarrow}$) between Fe and the multilayer structure via the formation of hybrid dual DSSs and Rashba states at the interface between Bi and Bi_2Se_3, as characterized by ARPES measurements. We note that where Bi is a 5d metal that is supposed to possess a strong spin−orbit coupling, the spin diffusion length of Bi measured by previous reports is quite long, exceeding more than 50 nm.[28] Thus, the increase in additional damping arising from the bulk contribution of Bi can be ruled out.

Spin Pumping and Inverse Edelstein Effect. Figure 3d shows the obtained transverse voltage signal as a function of magnetic field in Fe/MgO, Fe/Bi/Al_2O_3, Fe/Bi_2Se_3/$SrTiO_3$, Fe/Bi(1BL)/Bi_2Se_3/$SrTiO_3$, Fe/Bi(3BL)/Bi_2Se_3/$SrTiO_3$, and Fe/Bi(7BL)/Bi_2Se_3/ $SrTiO_3$ samples, respectively. The sign of the measured voltage response reverses when the direction of the magnetic field is reversed from $\theta = 0°$ to 180° (see the spin pumping setup in Figure 3a), as expected from IEE in the Rashba and TI systems.[4,10] In addition to the IEE voltage arising from the injected spin current via spin pumping, the measured V_{SP} may contain contributions from possible anisotropic magnetoresistance (AMR), anomalous Hall effect (AHE), and/or planar Hall effect (PHE) responses from the FM layer,[29] which can be separated (see the Supporting Information). The actual IEE-induced voltage signal (V_{IEE}) is calculated from $V_{IEE} = [V_S(+H) - V_S(-H)]/2$ by eliminating possible Seebeck-related voltage signals.

We found the following: (i) A null voltage response in the Fe/MgO sample (without Bi or Bi_2Se_3) excludes the spin rectification effects from the Fe layer. (ii) The measured voltage response in the Fe/Bi/Al_2O_3 sample is negligible, indicating that the bulk ISHE contribution from the Bi layer can be ruled out.[10] (iii) All the devices with Bi_2Se_3 multilayered structures show sizable V_{IEE} responses at room temperature. The positive sign of the voltage response at positive magnetic field indicates that a positive polarity of the IEE conversion arises from the clockwise spin texture with left-handed helicity.[4,30] Remarkably, the obtained V_{IEE} value does not follow a simple monotonic change (increase or decrease)

DOI: 10.1021/acs.nanolett.9b01151
Nano Lett. 2019, 19, 4420−4426

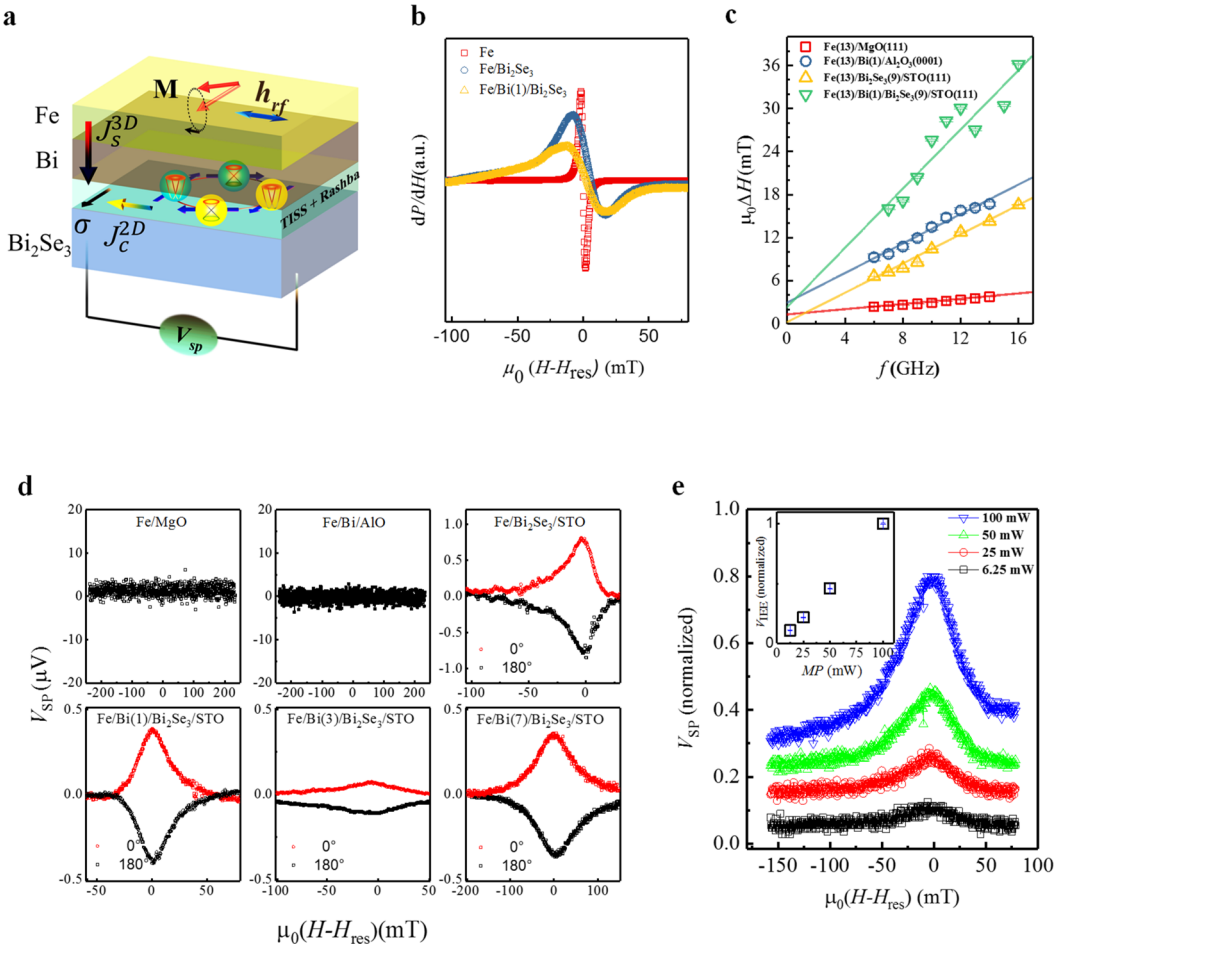

Figure 3. (a) Schematic of the experimental setup for spin pumping measurements on the Fe/Bi(d)/Bi_2Se_3 sample at room temperature, where d is the thickness of the Bi bilayer. (b, c) Comparison of the FMR absorption derivative vs magnetic field H measured at 11 GHz and half-maximum line width of the FMR spectrum as a function of microwave frequency, respectively. The solid lines show the linear fitting, from which the damping factor (α) of each sample is derived. (d) Magnetic field (H) dependence of IEE responses for Fe/MgO, Fe/Al_2O_3, Fe/Bi(1BL)/Bi_2Se_3, Fe/Bi(3BL)/Bi_2Se_3, and Fe/Bi(7BL)/Bi_2Se_3 at 300 K. The obtained voltage signal reverses its polarity when the direction of the magnetic field is reversed (the red and black curves correspond to the measurement under the positive and negative magnetic field, respectively). The microwave power was 50 mW, and the frequency was fixed at 14 GHz. (e) $V_{SP}(H)$ plot of the Fe/Bi(1BL)/Bi_2Se_3 sample under the microwave power of 6, 25, 50, and 100 mW (black, red, green, and blue curves, respectively). The $V_{SP}(H)$ plots at different power are shifted for clarification. The inset shows the obtained IEE voltage signal (after subtracting the AHE component using equation S3, see the Supporting Information) as a function of microwave power.

as a function of Bi thickness; namely, a larger V_{IEE} response is observed in the Fe/Bi(5,7BL)/Bi_2Se_3(9QL) sample whereas a much smaller value is observed in the Fe/Bi(2,3BL)/Bi_2Se_3(9QL) sample. Earlier studies showed that the top and bottom surface state of the Bi_2Se_3 thin film with opposite spin polarization would be decoupled when the thickness of Bi_2Se_3 is above 6 QL, resulting in a constant value of IEE coefficient via TISS at higher QLs.[4] Thus, the variation of V_{IEE} response (characterized by the IEE length, see discussion below) as a function of Bi thickness suggests that there would be another mechanism that plays a key role in determining the interfacial spin-momentum locking efficiency at the Bi/Bi_2Se_3 interface.

Figure 3e shows the measured V_{SP}(H) response of Fe/Bi(1BL)/Bi_2Se_3(9QL) as a function of microwave powers at the excitation frequency of 14 GHz. The inset of Figure 3e shows a linear plot of the microwave power dependence of V_{IEE}, as expected from the mechanism of spin pumping.

Thickness Dependence of IEE Length. To obtain the IEE length from the experimental data, we used a standard analysis of the spin pumping model to obtain the injected vertical spin current density (J_s^{3D}) (see the Supporting Information) generated by magnetization precession in the ferromagnetic (FM) layer and the resulted 2D transverse charge current density (J_c^{2D}). The charge density J_c^{2D} in our samples (sample width w = 2.5 mm, length l = 5 mm, and waveguide stripe line width L = 0.2 mm) is calculated by $J_c^{2D} = \frac{V_{IEE}(\sigma_{Fe}d_{Fe} + \sigma_{BiSe}d_{BiSe} + \sigma_{Bi}d_{Bi})}{(d_{Fe} + d_{Bi} + d_{BiSe})L}$, where σ_{Fe}, σ_{BiSe}, σ_{Bi}, d_{Fe}, d_{BiSe}, and d_{Bi} represent the electron conductivity and the thickness of bulk Fe, Bi_2Se_3, and Bi, respectively.

Figure 4a,b shows the obtained damping factor and IEE length as a function of Bi thickness in the multilayer structures. The damping factor increases from ~0.03 (d_{Bi} = 0BL) to 0.14 (d_{Bi} = 5BL) when the Bi thickness is increased. The spin mixing conductance ($g_{eff}^{\uparrow\downarrow}$) (inset of Figure 4a) in the Fe/Bi(5BL)/Bi_2Se_3 sample related to the enhancement of the damping factor is found to be ~16.57×10^{20} m^{-2}, which is 8 times higher than that in the Fe/Bi_2Se_3 sample without the Bi interlayer. Interestingly, $\lambda_{IEE}(d_{Bi})$ does not follow the similar trend. After the initial increase of λ_{IEE} (~155.0 pm) at the first

DOI: 10.1021/acs.nanolett.9b01151
Nano Lett. 2019, 19, 4420−4426

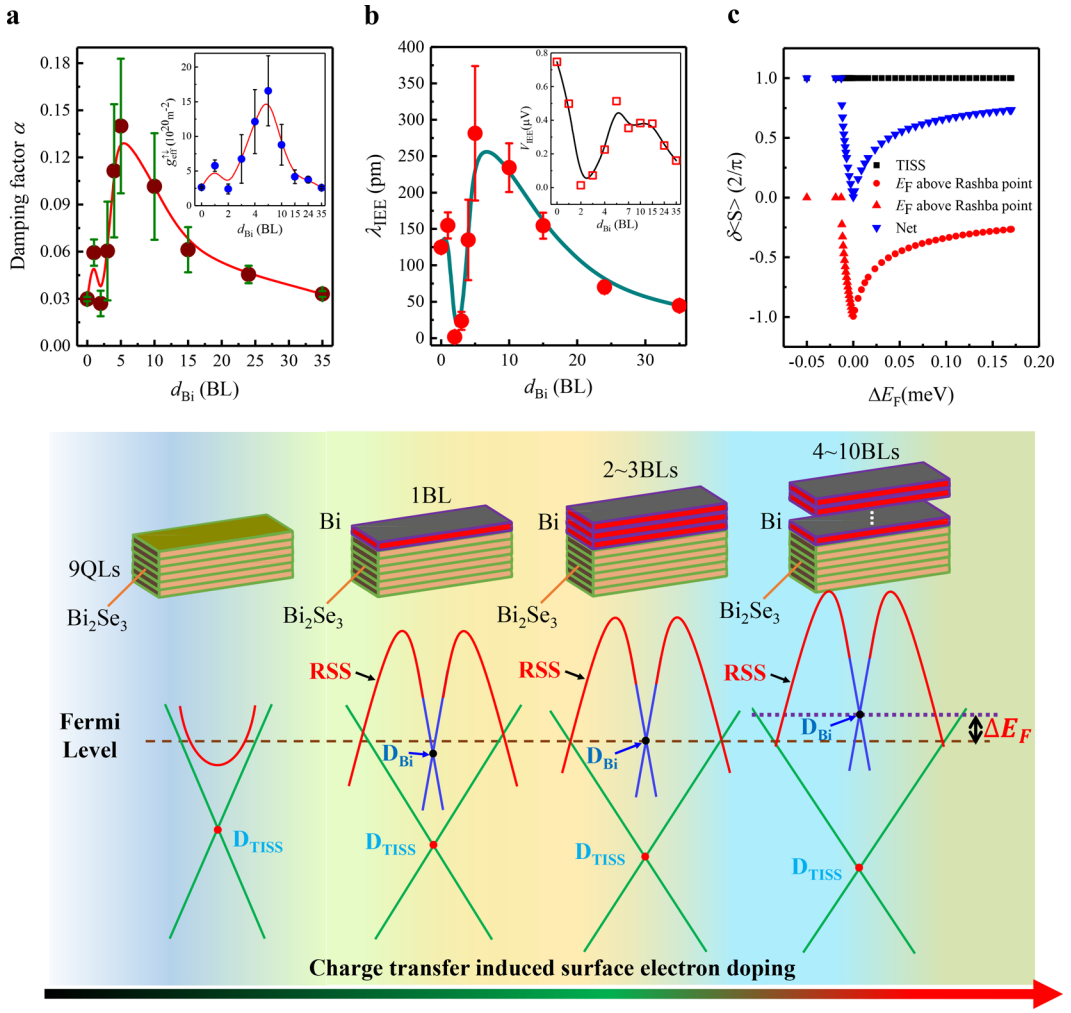

Figure 4. (a) Obtained damping factor and spin mixing conductance ($g_{eff}^{\uparrow\downarrow}$, inset). (b) Obtained IEE voltage (inset) and spin-to-charge conversion ratio via IEE (the length of λ_{IEE}) as a function of Bi thickness. (c) Relationship between average spin polarization $\delta\langle S\rangle$ and Fermi level shift ΔE_F for TISS, Rashba, and their combined states ($\Delta E_F = E_D - E_F$). The bottom panel shows a schematic for energy band evolution and Fermi level location corresponding to dual Dirac states and Rashba states.

Bi bilayer, the value of λ_{IEE} drops dramatically at d_{Bi} = 2BL (~2 pm), which is 2 orders of magnitude smaller than that in the Fe/Bi_2Se_3 sample (~124.8 pm). The obtained value of λ_{IEE} in the prepared Fe/Bi_2Se_3 sample is larger than a previously reported value of about 35 pm[4] and 70 pm in Py/$(Bi,Sb)_2Te_3$.[22] It is noted that, in previously reported FM/TI systems (YIG/Bi_2Se_3 (0.4×10^{19} m^{-2})[4] and Py/$(Bi,Sb)_2Te_3$ (1.0×10^{19} m^{-2})[22]), the obtained values of the spin mixing conductance are orders of magnitude smaller than in our results. The enhanced spin mixing conductance in the Fe/Bi (5BL)/Bi_2Se_3 sample suggests that much spin dissipation occurred at the interface due to the coexistence of Rashba surface states and TISS. A significant enhancement of λ_{IEE} up to ~281.4 pm was achieved with the continued further increasing of the Bi thickness, with a maximum at 5BL.

The observed Bi thickness-dependent λ_{IEE} cannot be attributed to a simple TISS state from the top-QL Bi_2Se_3, in which the spin-to-charge conversion would remain unchanged when Bi_2Se_3 is above 6QL.[4] The bulk ISHE contribution from the Bi interlayer can also be excluded since no pronounced signal is observed in the Fe/Bi/Al_2O_3 sample. Moreover, there is no observed Rashba-split band in the bulk conduction band of the Bi_2Se_3 induced by the top Bi layer, in contrast to the case of nonmagnetic metal Ag on Bi_2Se_3.[31] We note that spin accumulation is an indispensable part of bridging the interconversion of spin current and charge current, and the magnitude of the effective spin accumulation determines the efficiency of spin−charge conversion but depends on the value of the spin polarization potential. The spin polarization potential was defined as $\delta\left\langle \vec{S} \right\rangle = \frac{\sum_i \delta\langle\vec{S}_i\rangle \mathrm{DOS}_i}{\sum_i \mathrm{DOS}_i}$, where $\delta\langle\vec{S}\rangle$ and DOS_i are the spin polarization potential and density of states average for a given channel index.[20] A recent numerical calculation shows that, under a multichannel scattering condition where Rashba states exist, the spin polarization potential induced by charge current can be energy-dependent.[20] That means that the λ_{IEE} can be tuned by changing the Fermi level, which provides us with an effective model to explain our results, shown in Figure 4c. Therefore, the change of the spin-to-charge conversion coefficient would be attributed to a synergistic effect induced by hybrid TISS and Rashba spin-splitting states occurring at the 2D Bi/Bi_2Se_3 interface.

From the energy dispersions characterized by ARPES, there are four distinct near-circular Fermi contours with opposite spin helicity: the interfacial Rashba-split bands ("1" and "2"),

DOI: 10.1021/acs.nanolett.9b01151
Nano Lett. 2019, 19, 4420−4426

the first DSS with topological protection band ("3") from the top-QL Bi_2Se_3, and the second DSS band ("4") from the Bi surface state. While the DSSs from the top-QL Bi_2Se_3 or Bi/Bi_2Se_3 interface produce an energy-independent positive spin polarization, the Rashba-split bands will yield an opposite sign of spin polarization which is energy-dependent;[20] namely, its spin polarization is maximum near the crossing point of the Rashba-split bands and decreases as the energy level increases. Combined with these three types of spin textures, the overall net spin polarization strongly depends on the location of the Fermi level, as shown in Figure 4c. In principle, each contour can convert the injected 3D spin current into a 2D charge current via IEE individually (the direct coupling between Fermi contours is ignored to simplify the analysis), resulting in a change of spin-to-charge conversion (i.e., λ_{IEE}) as a function of Fermi level, elevated by the charge transfer effect from the added Bi bilayers. The net IEE response in the multilayered structures could be expressed as a sum of three IEE terms:[32]

$$\lambda_{net} = \lambda_{Bi_2Se_3(TISS)} + \lambda_{Bi(DSS)} + \lambda_{Bi(Rashba)} = \nu_F^{D_{Bi_2Se_3}} \tau_s^{D_{Bi_2Se_3}} + \nu_F^{D_{Bi}} \tau_s^{D_{Bi}} + \frac{\alpha_R(E_F)}{\hbar} \tau_s^{R} \quad (1)$$

where $\nu_F^{D_{Bi}}$ ($+4.4 \times 10^5$ m/s) and $\nu_F^{D_{Bi2Se3}}$ ($+3.81 \times 10^5$ m/s) are the Fermi velocity of the TISS in Bi and Bi_2Se_3, respectively. As mentioned above, for a simple approximation, as long as the Rashba strength and spin-momentum scattering time are given, the IEE length should be fixed, but in fact the spin polarization potential can be tuned according to the Fermi level location due to the Fermi velocity changes in each splitting band. The red dots in Figure 4c show the variations of spin polarization in Rashba states with the shifting of the Fermi level, while in the Dirac states it stays constant (black line in Figure 4c). It is at its minimum when the Fermi level intersects the cross points of the Rashba-split bands, corresponding to the minimum λ_{IEE} at 2−3BLs. As electrons transfer into the Bi_2Se_3 layer, the Fermi level shifts down relative to the Rashba bands and up relative to the D_{TISS}. Thus, the compensated spin polarization from Rashba states decays sharply while the IEE length increases rapidly at 4−10BLs, and consequently there is a recovery of the IEE length in thinner bismuth layers. With thicker Bi bilayers, a portion of the spin current is dissipated in the Bi layer, resulting in a decay of the IEE length. These processes are illustrated in Figure 4, bottom panel.

In summary, we observed a tunable IEE response by varying the thickness of a Bi bilayer on top of a Bi_2Se_3 layer. The ARPES experiments confirmed the formation of a 2DEG and the developed second Dirac cone and Rashba-split bands, which is attributed to topological proximity in the Bi/Bi_2Se_3 hybrid together with nontrivial intrinsic spin−orbit interactions. By performing spin pumping measurements, we unravel a relationship between the spin-to-charge conversion and the interfacial electronic structure at the Bi/Bi_2Se_3 interface by tuning the Fermi level, suggesting that the synergistic contributions of the dual Dirac surface states and emergent Rashba-split states dominate the spin-to-charge conversion in the multilayer Bi/Bi_2Se_3 system. Our work provides compelling opportunities for the next generation of Bi/van der Waals and TI-based spintronics, paving a promising pathway to achieve a high spin-to-charge conversion coefficient by tailoring the strong spin−orbit coupling interface.

■ ASSOCIATED CONTENT

Supporting Information

The Supporting Information is available free of charge on the ACS Publications website at DOI: 10.1021/acs.nanolett.9b01151.

Bi_2Se_3 and Bi/Bi_2Se_3 thin films growth and characterization; details of the ARPES, FMR, and spin pumping experiments (PDF)

■ AUTHOR INFORMATION

Corresponding Authors

*E-mail: dsun4@ncsu.edu.
*E-mail: zhcheng@iphy.ac.cn.

ORCID

Rui Sun: 0000-0001-7006-2133
Xu Yang: 0000-0001-9687-9424

Author Contributions

Zhao-hua Cheng, Dali Sun, and Rui Sun conceived this study and the experiments. Rui Sun fabricated the devices. Rui Sun and Xu Yang measured the ARPES. Eric Vetter and Shi-jia Yang measured the FMR, spin pumping, and calibrated rf field. Na Li and Lei Su helped measure the AFM and XRD. Yan Li, Zi-zhao Gong, Yang Li, Zong-kai Xie, Kai-yue Hou, and Qeemat Gul helped with sample growths and MBE operations. Wei He and Xiang-qun Zhang made contributions to the MBE and ARPES setup. Rui Sun, Dali Sun, and Zhao-hua Cheng wrote the paper. Dali Sun and Zhao-hua Cheng were responsible for the project planning and group managing. All authors discussed the results and worked on data analysis and manuscript preparation.

Notes

The authors declare no competing financial interest.

■ ACKNOWLEDGMENTS

This work is supported by the National Key Research Program of China (Grants 2015CB921403, 2016YFA0300701, and 2017YFB0702702), the National Natural Sciences Foundation of China (Grants 1187411, 91622126, 51427801, and 51671212), and the Key Research Program of Frontier Sciences, CAS (Grants QYZDJ-SSW-JSC023, KJZD-SW-M01, and ZDYZ2012-2). Eric Vetter, Shi-jia Yang, and Dali Sun are grateful for support from the startup provided by North Carolina State University.

■ REFERENCES

(1) Hsieh, D.; Xia, Y.; Qian, D.; Wray, L.; Dil, J. H.; Meier, F.; Osterwalder, J.; Patthey, L.; Checkelsky, J. G.; Ong, N. P.; Fedorov, A. V.; Lin, H.; Bansil, A.; Grauer, D.; Hor, Y. S.; Cava, R. J.; Hasan, M. Z. A tunable topological insulator in the spin helical Dirac transport regime. *Nature* **2009**, *460*, 1101−1105.

(2) Hasan, M. Z.; Kane, C. L. Colloquium: Topological insulators. *Rev. Mod. Phys.* **2010**, *82*, 3045−3067.

(3) Mellnik, A. R.; Lee, J. S.; Richardella, A.; Grab, J. L.; Mintun, P. J.; Fischer, M. H.; Vaezi, A.; Manchon, A.; Kim, E. A.; Samarth, N.; Ralph, D. C. Spin-transfer torque generated by a topological insulator. *Nature* **2014**, *511*, 449−451.

(4) Wang, H.; Kally, J.; Lee, J. S.; Liu, T.; Chang, H.; Hickey, D. R.; Mkhoyan, K. A.; Wu, M.; Richardella, A.; Samarth, N. Surface-State-Dominated Spin-Charge Current Conversion in Topological-Insulator-Ferromagnetic-Insulator Heterostructures. *Phys. Rev. Lett.* **2016**, *117*, 076601.

DOI: 10.1021/acs.nanolett.9b01151
Nano Lett. 2019, 19, 4420−4426

(5) Shen, K.; Vignale, G.; Raimondi, R. Microscopic theory of the inverse Edelstein effect. *Phys. Rev. Lett.* **2014**, *112*, 096601.
(6) Rojas-Sanchez, J.-C.; Oyarzún, S.; Fu, Y.; Marty, A.; Vergnaud, C.; Gambarelli, S.; Vila, L.; Jamet, M.; Ohtsubo, Y.; Taleb-Ibrahimi, A.; Le Fevre, P.; Bertran, F.; Reyren, N.; George, J.-M.; Fert, A. Spin to Charge Conversion at Room Temperature by Spin Pumping into a New Type of Topological Insulator: α-Sn Films. *Phys. Rev. Lett.* **2016**, *116*, 096602.
(7) Fan, Y.; Kou, X.; Upadhyaya, P.; Shao, Q.; Pan, L.; Lang, M.; Che, X.; Tang, J.; Montazeri, M.; Murata, K.; Chang, L.; Akyol, M.; Yu, G.; Nie, T.; Wong, K.; Liu, J.; Wang, Y.; Tserkovnyak, Y.; Wang, K. L. Electric-field control of spin−orbit torque in a magnetically doped topological insulator. *Nat. Nanotechnol.* **2016**, *11*, 352−359.
(8) Han, W.; Otani, Y.; Maekawa, S. Quantum materials for spin and charge conversion. *Npj Quantum Mater.* **2018**, *3*, 27.
(9) Manchon, A.; Koo, H. C.; Nitta, J.; Frolov, S. M.; Duine, R. A. New perspectives for Rashba spin-orbit coupling. *Nat. Mater.* **2015**, *14*, 871−882.
(10) Sánchez, J. C. R.; Vila, L.; Desfonds, G.; Gambarelli, S.; Attané, J. P.; De Teresa, J. M.; Magén, C.; Fert, A. Spin-to-charge conversion using Rashba coupling at the interface between non-magnetic materials. *Nat. Commun.* **2013**, *4*, 2944.
(11) King, P. D. C.; Hatch, R. C.; Bianchi, M.; Ovsyannikov, R.; Lupulescu, C.; Landolt, G.; Slomski, B.; Dil, J. H.; Guan, D.; Mi, J. L.; Rienks, E. D. L.; Fink, J.; Lindblad, A.; Svensson, S.; Bao, S.; Balakrishnan, G.; Iversen, B. B.; Osterwalder, J.; Eberhardt, W.; Baumberger, F.; Hofmann, Ph. Large Tunable Rashba Spin Splitting of a Two-Dimensional Electron Gas in Bi_2Se_3. *Phys. Rev. Lett.* **2011**, *107*, 096802.
(12) Zhu, Z. H.; Levy, G.; Ludbrook, B.; Veenstra, C. N.; Rosen, J. A.; Comin, R.; Wong, D.; Dosanjh, P.; Ubaldini, A.; Syers, P.; Butch, N. P.; Paglione, J.; Elfimov, I. S.; Damascelli, A. Rashba Spin-Splitting Control at the Surface of the Topological Insulator Bi_2Se_3. *Phys. Rev. Lett.* **2011**, *107*, 186405.
(13) Hirahara, T.; Fukui, N.; Shirasawa, T.; Yamada, M.; Aitani, M.; Miyazaki, H.; Matsunami, M.; Kimura, S.; Takahashi, T.; Hasegawa, S.; Kobayashi, K. Atomic and electronic structure of ultrathin Bi(111) films grown on Bi_2Te_3(111) substrates: Evidence for a strain-induced topological phase transition. *Phys. Rev. Lett.* **2012**, *109*, 227401.
(14) Song, K.; Soriano, D.; Cummings, A. W.; Robles, R.; Ordejon, P.; Roche, S. Spin Proximity Effects in Graphene/Topological Insulator Heterostructures. *Nano Lett.* **2018**, *18*, 2033−2039.
(15) Wang, T.-H.; Jeng, H.-T. Wide-range ideal 2D Rashba electron gas with large spin splitting in $Bi_2Se_3/MoTe_2$ heterostructure. *Npj. Comp. Mater.* **2017**, *3*, 5.
(16) Fleet, L. Bismuth: Not a trivial matter. *Nat. Phys.* **2017**, *13*, 8−8.
(17) Shoman, T.; Takayama, A.; Sato, T.; Souma, S.; Takahashi, T.; Oguchi, T.; Segawa, K.; Ando, Y. Topological proximity effect in a topological insulator hybrid. *Nat. Commun.* **2015**, *6*, 6547.
(18) Su, S. H.; Chuang, P. Y.; Chen, S. W.; Chen, H. Y.; Tung, Y.; Chen, W.; Wang, C.; Yang, Y.; Huang, J. C. A.; Chang, T.; Lin, H.; Jeng, H.; Cheng, C.; Tsuei, K.; Su, H.; Wu, Y. C. Selective Hydrogen Etching Leads to 2D Bi(111) Bilayers on Bi_2Se_3: Large Rashba Splitting in Topological Insulator Heterostructure. *Chem. Mater.* **2017**, *29*, 8992−9000.
(19) Ast, C. R.; Henk, J.; Ernst, A.; Moreschini, L.; Falub, M. C.; Pacile, D.; Bruno, P.; Kern, K.; Grioni, M. Giant spin splitting through surface alloying. *Phys. Rev. Lett.* **2007**, *98*, 186807.
(20) Hong, S.; Diep, V.; Datta, S.; Chen, Y. P. Modeling potentiometric measurements in topological insulators including parallel channels. *Phys. Rev. B: Condens. Matter Mater. Phys.* **2012**, *86*, No. 085131.
(21) Miao, L.; Wang, Z. F.; Ming, W.; Yao, M. Y.; Wang, M.; Yang, F.; Song, Y. R.; Zhu, F.; Fedorov, A. V.; Sun, Z.; Gao, C. L.; Liu, C.; Xue, Q. K.; Liu, C. X.; Liu, F.; Qian, D.; Jia, J. F. Quasiparticle dynamics in reshaped helical Dirac cone of topological insulators. *Proc. Natl. Acad. Sci. U. S. A.* **2013**, *110*, 2758−2762.
(22) Mendes, J. B. S.; Alves Santos, O.; Holanda, J.; Loreto, R. P.; de Araujo, C. I. L.; Chang, C.-Z.; Moodera, J. S.; Azevedo, A.; Rezende, S. M. Dirac-surface-state-dominated spin to charge current conversion in the topological insulator $(Bi_{0.22}Sb_{0.78})_2Te_3$ films at room temperature. *Phys. Rev. B: Condens. Matter Mater. Phys.* **2017**, *96*, 180415R.
(23) Chen, J.; Qin, H. J.; Yang, F.; Liu, J.; Guan, T.; Qu, F. M.; Zhang, G. H.; Shi, J. R.; Xie, X. C.; Yang, C. L.; Wu, K. H.; Li, Y. Q.; Lu, L. Gate-Voltage Control of Chemical Potential and Weak Antilocalization in Bi_2Se_3. *Phys. Rev. Lett.* **2010**, *105*, 176602.
(24) Lee, J.; Park, J.; Lee, J.-H.; Kim, J. S.; Lee, H.-J. Gate-tuned differentiation of surface-conducting states in $Bi_{1.5}S_{0.5}Te_{1.7}Se_{1.3}$ topological-insulator thin crystals. *Phys. Rev. B: Condens. Matter Mater. Phys.* **2012**, *86*, 245321.
(25) Analytis, J. G.; Chu, J.-H.; Chen, Y.; Corredor, F.; McDonald, R. D.; Shen, Z. X.; Fisher, I. R. Bulk Fermi surface coexistence with Dirac surface state in Bi_2Se_3: A comparison of photoemission and Shubnikov–de Haas measurements. *Phys. Rev. B: Condens. Matter Mater. Phys.* **2010**, *81*, 205407.
(26) Chang, C. Z.; Tang, P.; Feng, X.; Li, K.; Ma, X. C.; Duan, W.; He, K.; Xue, Q. K. Band Engineering of Dirac Surface States in Topological-Insulator-Based van der Waals Heterostructures. *Phys. Rev. Lett.* **2015**, *115*, 136801.
(27) Eich, A.; Michiardi, M.; Bihlmayer, G.; Zhu, X. G.; Mi, J. L.; Iversen, Bo B.; Wiesendanger, R.; Hofmann, Ph; Khajetoorians, A. A.; Wiebe, J. Intra- and interband electron scattering in a hybrid topological insulator: Bismuth bilayer on Bi_2Se_3. *Phys. Rev. B: Condens. Matter Mater. Phys.* **2014**, *90*, 155414.
(28) Hou, D.; Qiu, Z.; Harii, K.; Kajiwara, Y.; Uchida, K.; Fujikawa, Y.; Nakayama, H.; Yoshino, T.; An, T.; Ando, K.; Jin, X.; Saitoh, E. Interface induced inverse spin Hall effect in bismuth/permalloy bilayer. *Appl. Phys. Lett.* **2012**, *101*, 042403.
(29) Deorani, P.; Son, J.; Banerjee, K.; Koirala, N.; Brahlek, M.; Oh, S.; Yang, H. Observation of inverse spin Hall effect in bismuth selenide. *Phys. Rev. B: Condens. Matter Mater. Phys.* **2014**, *90*, 094403.
(30) Kondou, K.; Yoshimi, R.; Tsukazaki, A.; Fukuma, Y.; Matsuno, J.; Takahashi, K. S.; Kawasaki, M.; Tokura, Y.; Otani, Y. Fermi-level-dependent charge-to-spin current conversion by Dirac surface states of topological insulators. *Nat. Phys.* **2016**, *12*, 1027−1031.
(31) Shi, S.; Wang, A.; Wang, Y.; Ramaswamy, R.; Shen, L.; Moon, J.; Zhu, D.; Yu, J.; Oh, S.; Feng, Y.; Yang, H. Efficient charge-spin conversion and magnetization switching through the Rashba effect at topological-insulator/Ag interfaces. *Phys. Rev. B: Condens. Matter Mater. Phys.* **2018**, *97*, 041115R.
(32) Lesne, E.; Fu, Y.; Oyarzun, S.; Rojas-Sanchez, J. C.; Vaz, D. C.; Naganuma, H.; Sicoli, G.; Attane, J. P.; Jamet, M.; Jacquet, E.; George, J.-M.; Barthelé my, A.; Jaffre´ s, H.; Fert, A.; Bibes, M.; Vila, L. Highly efficient and tunable spin-to-charge conversion through Rashba coupling at oxide interfaces. *Nat. Mater.* **2016**, *15*, 1261−1266.

DOI: 10.1021/acs.nanolett.9b01151
Nano Lett. 2019, 19, 4420−4426